Efficient Transparent Thin Dye Solar Cells Based on Highly Porous 1D Photonic Crystals

Silvia Colodrero, Amparo Forneli, Carmen López-López, Laia Pellejà, Hernán Míguez, and Emilio Palomares**

A working electrode design based on a highly porous 1D photonic crystal structure that opens the path towards high photocurrents in thin, transparent, dye-sensitized solar cells is presented. By enlarging the average pore size with respect to previous photonic crystal designs, the new working electrode not only increases the device photocurrent, as predicted by theoretical models, but also allows the observation of an unprecedented boost of the cell photovoltage, which can be attributed to structural modifications caused during the integration of the photonic crystal. These synergic effects yield conversion efficiencies of around 3.5% by using just 2 μm thick electrodes, with enhancements between 100% and 150% with respect to reference cells of the same thickness.

1. Introduction

Dye sensitized solar cells (DSSCs) with efficiencies up to 11% can already be prepared on a laboratory scale.[1–3] However, in most cases, these high performance devices are still constructed using thick TiO_2 mesoporous films made of crystalline nanoparticles (15–20 nm) plus an additional (≈4 μm thick) diffuse scattering layer composed of larger particles,[4–9] typically with diameters on the order of the hundreds of nanometers, which prevents the solar cells from being transparent. Thus, alternatives to this scatter layer should be explored for those applications in which transparency is needed. Different approaches that do not turn the cell opaque are being explored to boost the photocurrent or the photovoltage of DSSCs. Among them, we point out the design of new dyes of wider spectral absorption,[3,10,11] which yields an increase of the photocurrent and whose effect over the interfacial charge transfer reactions is currently being analyzed.[12] In fact, major steps have been achieved recently by using either polythiophene organic dyes[13] or thiophene-containing bipyridine ligands that are used in heteroleptic ruthenium complexes.[14,15] The use of the thiophene unit has allowed increasing the sensitizer molecular extinction coefficient[16] and, therefore, decreasing the TiO_2 mesoporous working electrode thickness, with the concurrent increase in the device open circuit voltage (V_{OC}), without diminishing the cell photocurrent density (J_{SC}). Strategies based on molecular energy transfer relays included in the electrolyte composition have been also studied as a pathway to increase the photocurrent but with a parallel decrease on the cell voltage.[17] Yet, further improvement requires that new concepts be applied to the mesoporous metal oxide working electrode.[18]

In 2003, in a seminal paper by T. Mallouk and co-workers, the optical absorption enhancement effect of porous photonic structures integrated in DSSCs was demonstrated for the first time.[19] In that work, the working electrode was built by coupling a standard 7 μm nanocrystalline titanium oxide (nc-TiO_2) layer to a thick (4 μm) 3D photonic structure of low optical quality, which gave rise to both directional and diffuse scattering phenomena. The proof of this concept, which has been deeply analyzed and confirmed,[20–23] encouraged new attempts to use other metal oxide photonic structures with more robust structural and optical properties that allow for a fine control of light absorption in the cell.

It was previously demonstrated that a thin (≈500 nm) nanoparticle based 1D photonic crystal (1DPC) coupled to a dyed mesoporous TiO_2 layer could give rise to significant increases of the device short circuit photocurrent ($15\% < J_{SC} < 30\%$), which yields an increase of the power conversion efficiency ranged between $10\% < \eta < 25\%$ when measured at high and low illumination levels, respectively.[24] Such 1D photonic lattices showed no diffuse scattering, which allowed one to attain, for the first time, devices of enhanced efficiency while preserving the transparency, which is a topic of major interest due to their possible application for building integrated photovoltaics (BIPV). However, the achieved photocurrents were not very high. Although this could be partly due to the low number of layers the Bragg mirror was made of, which limited its specular reflectance within the cell,[25] the observed simultaneous photovoltage and fill factor decrease with the presence of the multilayer indicated that there might be electrolyte diffusion problems through the photonic structure. Also, prior attempts

S. Colodrero, C. López-López, Dr. H. Míguez
Instituto de Ciencia de Materiales de Sevilla (CSIC-US)
Centro de Investigaciones Científicas Isla de la Cartuja
C/Américo Vespucio 49, 41092 Sevilla, Spain
E-mail: hernan@icmse.csic.es
A. Forneli, L. Pellejà, Dr. E. Palomares
Institute of Chemical Research of Catalonia (ICIQ) Avda. Països Catalans 16, 43007 Tarragona, Spain
E-mail: epalomares@iciq.es
Dr. E. Palomares
Institució Catalana de Recerca i Estudis Avançats (ICREA)
Avda. Lluís Companys 23, 08010 Barcelona, Spain

DOI: 10.1002/adfm.201102159

to boost the performance of very thin cells using similar 1DPCs resulted in very low absolute values of the efficiency.[26]

Here, we show that by means of coupling newly designed nanoparticle-based 1DPCs of increased porosity to the working electrode a simultaneous increase in both photocurrent and photovoltage can be achieved, which boosts the conversion efficiency of thin cells up to unprecedented values that are close to those typically observed for much thicker cells. At the same time, we show that the photonic crystals perform like light harvesting enhancers, approximately as good as the widely employed diffuse scattering layers, provided their thickness is on the same order of magnitude, but maintain one of the primary added values of the original cell: its transparency. Our approach is based on the gradual incorporation of polymeric porogenes to the multilayer while being deposited on the standard nc-TiO_2 electrode, which allow us to enlarge the pore size of the photonic crystal and to preserve the optical quality at the same time, leading to improved flow of electrolyte through it. An increase in the photovoltage is also observed, which is attributed to the concomitant formation of a thin insulating layer on the titania nanocrystals during the deposition of the photonic crystal, as supported by recombination lifetime measurements.[27] These synergic effects yield conversion efficiencies of ≈3.5% using 2 μm thick electrodes, with enhancements between 100% and 150% with respect to reference cells of the same thickness.

2. Results and Discussion

2.1. Structural Analysis of 1DPCs Coupled to DSSCs

In order to evaluate and compare the performance of DSSCs based on different types of light harvesting structures, namely 1DPC and diffuse scattering layers, a set of 5 μm thick transparent nc-TiO_2 electrodes was prepared. The set was used to investigate the effect that the presence of a more open void network in the photonic crystal had on the cell characteristics. We employed a method based on the addition and later removal of a polymeric porogen to the TiO_2 nanoparticle precursor suspension, which allowed us to increase significantly porosity and average pore size.

Prior to integration in the cell, a thorough study of the porosity of the nanoparticle layers forming the photonic crystal was realized by specular reflectance porosimetry, a technique that has been successfully employed before to characterize the vapor sorption properties of mesoporous multilayers.[28] Analysis of gas adsorption–desorption isotherms allowed us to attain pore size distribution curves such as those displayed in **Figure 1**a. In these plots, the ratio between the volume occupied by pores of a certain diameter and the total pore volume of the structure is plotted for layers of SiO_2 and TiO_2 nanoparticles (squares and circles, respectively), and for a layer of TiO_2 with enhanced pore size deposited from a mixture of TiO_2 nanoparticles and a sacrificial polymer (stars). It can be clearly seen that the originally employed colloidal suspensions gave rise to thin deposits of very different pore distribution and average size for both silica and titania particles, with much larger pores being present in the former than in the latter. After inclusion and removal of the polymer, the average pore size of the treated TiO_2 layers shifts from the original 15 nm to above 25 nm.

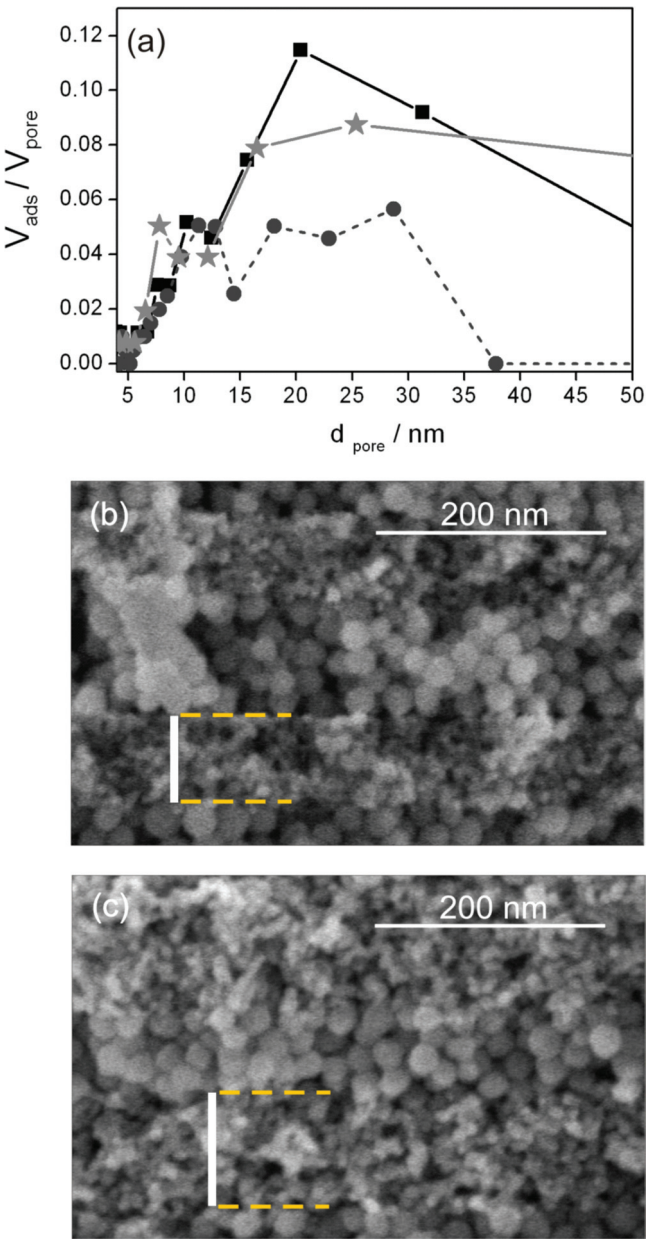

Figure 1. a) Pore size distributions attained from the analysis of isopropanol adsorption–desorption isotherms of layers of SiO_2 nanoparticles (squares), TiO_2 nanoparticles (circles), and a mixture of TiO_2 nanoparticles and polyethylene glycol after removal of the polymer (stars). b,c) FESEM cross sections of nanoparticle-based photonic crystals built by alternate deposition of TiO_2 layers of b) standard or c) increased average pore size and spherical silica particles.

These large pores coexist with narrow ones that are still present between nanocrystals. These films with wider pores were devised to improve the flow of electrolyte when integrated in the solar cell while keeping the optical quality of the multilayer structures that integrate them. In Figure 1b,c, we show field-emission scanning electron microscopy (FESEM) images of cross sections of a nanoparticle based 1DPC and a similar multilayer in which larger pores have been introduced, respectively.

After removal of the polymer, very large pores can be seen, in addition to a widening of the layer thickness.

Then, highly reflecting photonic structures were built onto the nc-TiO_2 electrodes using both the originally employed and the new colloidal titania suspensions. The total thickness of both photonic crystal layers was adjusted to be the same by slightly modifying the concentration of the precursor suspensions used during the deposition process. Also the respective reflectance spectra displayed Bragg peaks of similar intensities and located at approximately the same spectral regions. A typical reflectance spectrum of a 1DPC coupled to a nanocrystalline electrode will be shown later. Similarly, the thickness of the diffuse scattering layer was chosen to be as close as possible to that of the periodic multilayer in order to minimize the contribution to the current due to the photoconductivity of the overlayer in the former case and, additionally, to establish an assessment of the relative optical performance of each type of scattering layer. A reference electrode of the exact same thickness but without coupling any kind of scattering layer was also prepared for the sake of comparison. FESEM images corresponding to cross sections of nc-TiO_2 electrodes coupled to both the diffuse scattering layer and the highly porous nanoparticle-based 1DPC are displayed in **Figure 2**a,b, respectively. Closer observations, as shown in Figure 2c,d, allow the reader to see the detailed structure of the diffuse reflector layer, in which disordered large TiO_2 particles (diameters between 150 nm and 250 nm) are mixed with photoconducting TiO_2 nanocrystals, and of the nanoparticle photonic crystal, which is made of alternate layers of SiO_2 (spherical particles) and TiO_2 (nanocrystals of irregular shape), respectively.

2.2. Comparative Performance of DSSCs Coupled to 1DPCs of Enhanced Porosity

Results showing the comparative analysis carried out for the above-mentioned devices are presented in **Figure 3**. The characteristic current–voltage (*I–V*) curves shown in Figure 3a exhibit the highest increase in photocurrent for the case in which the pore-size-enhanced nanoparticle-based 1DPC has been integrated in the DSSC (dark grey line), while the lowest increment obtained corresponds to the incorporation of the originally reported photonic structure (light grey line). It can be also observed that, although a slightly lower photovoltage and fill factor are achieved for the DSSC coupled to the highly porous 1DPC, the use of polymeric porogen during the photonic crystal fabrication causes the solar cell with such periodic structure to perform almost as well as the one based on the diffuse scattering layer (dashed line).

In order to study if the more efficient 1DPC-based cell in which the nc-TiO_2 electrode is coupled to a highly porous multilayer also shows an improved flow of the electrolyte species through it, we employ voltammetry to estimate the tri-iodide diffusion constants, *D*, for the different cells analyzed here. Voltammetry curves are presented in Figure 3b for the devices under consideration. We found that the presence of a more open void network, created after incorporation and removal of polymer in the photonic structure, facilitates the transport of embedded compounds. Whereas *D* increases from 19×10^{-8} cm^2 s^{-1} in the cell containing the standard nanoparticle 1DPC to 29×10^{-8} cm^2 s^{-1} in the cell in which the 1DPC with larger pores was integrated, values are around 60×10^{-8} cm^2 s^{-1} for both the reference and the diffuse scattering layer based cells.

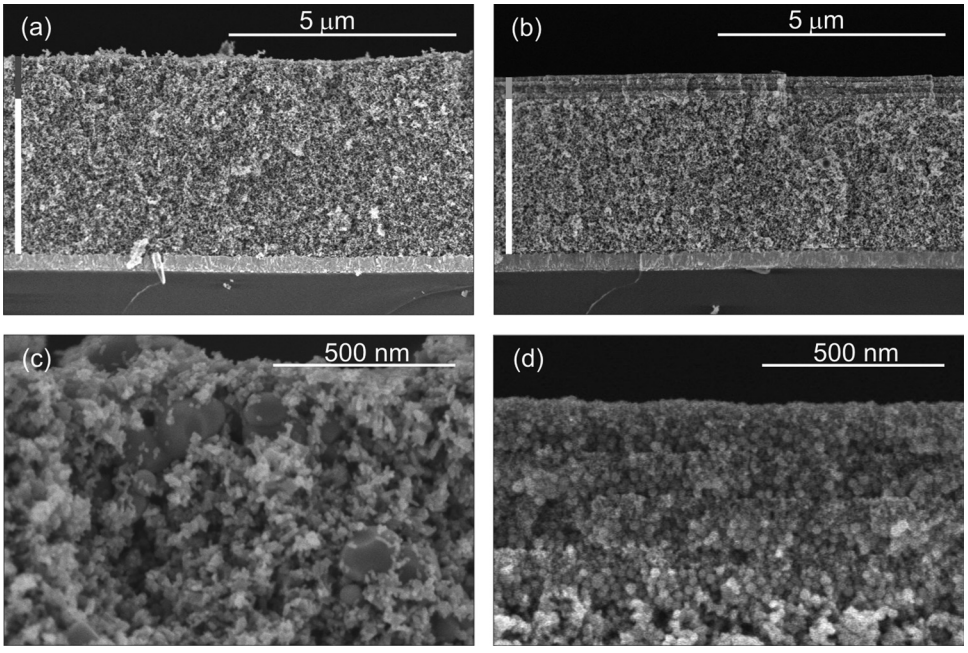

Figure 2. FESEM images of cross sections of an electrode made of nc-TiO_2 coupled to a) a diffuse scattering layer and b) a nanoparticle based 1DPC. High magnification images of the c) random and d) periodic photonic structures employed as scattering layers in each case are also shown. White bars indicate the width of the nc-TiO_2 electrode, while dark and light grey ones are as thick as the diffuse scattering layer and the photonic crystal layer, respectively.

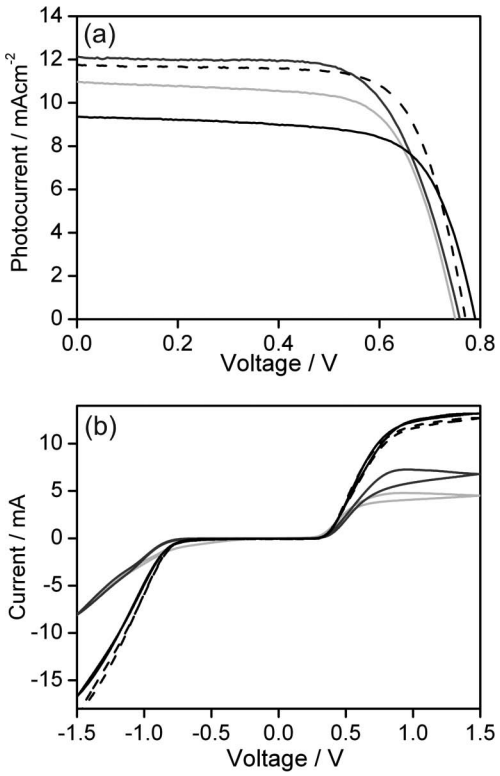

Figure 3. a) *I – V* and b) cyclic voltammetry curves measured for DSSCs in which a 5 µm thick nc-TiO_2 layer was coupled to a diffuse scattering layer (black dashed line), a non-modified 1DPC (light grey line), and a highly porous 1DPC (dark grey line). Results corresponding to a reference cell (black solid line) are also plotted for the sake of comparison.

These results indicate that, although the tri-iodide diffusion is still hindered to some extent, an undoubtedly improved transfer of charged species through the photonic crystal layer is obtained after enlargement of the pores, which correlated well with the observed enhancement of photocurrent.

2.3. Performance of Very Thin Electrodes Coupled to Highly Porous 1DPCs

After demonstrating the capability of highly porous 1DPCs to be used as light reflectors when integrated in DSSCs, we explored the effect of coupling the newly designed porous 1DPC to thin (2 µm thick) nc-TiO_2 electrodes, for which the enhancements are expected to be larger.[25] Because of the small width of the electrode, the contribution to the photocurrent resulting from the presence of dyed nc-TiO_2 within diffuse scattering layers could not be disregarded and no comparison with a DSSC based on this type of structure was carried out in this case. *I–V* and incident-photon-to-collected-electron (IPCE) efficiency results from a DSSC made of a 2 µm thick nc-TiO_2 active layer coupled to a highly porous 1DPC (grey line) are presented in **Figure 4**. For the sake of comparison, the performance of a reference cell with the same thickness of nc-TiO_2 layer, but without coupling the periodic structure, is also plotted (black line). As can be clearly seen in Figure 4a, there are two interesting effects

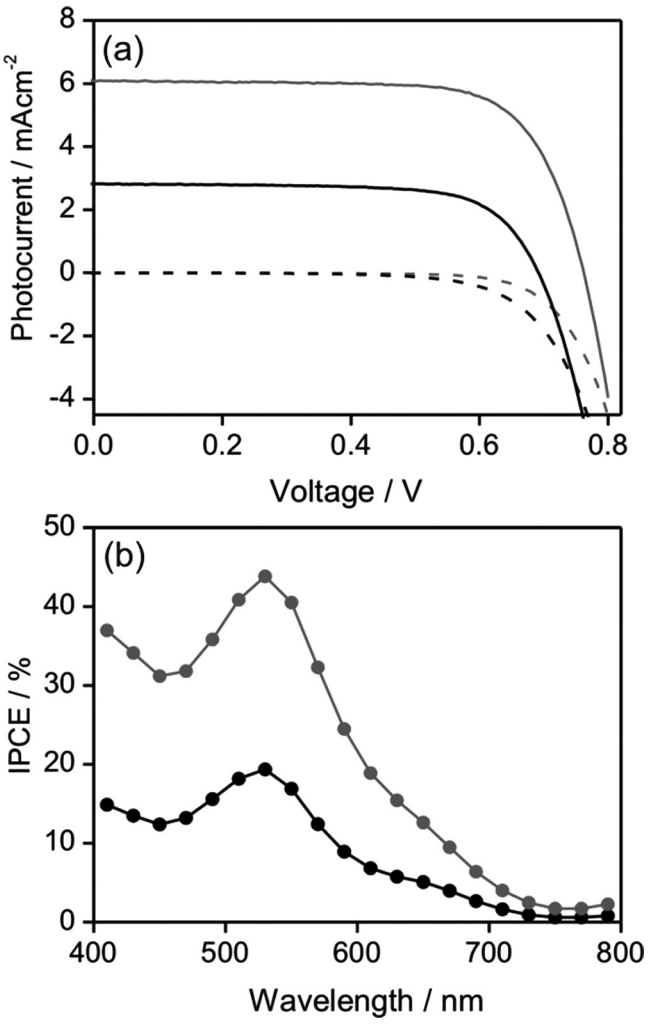

Figure 4. a) *I – V* and b) IPCE conversion efficiency curves for DSSCs in which a 2 µm thick nc-TiO_2 layer coupled to a highly porous 1DPC (grey line) and the same thickness of active TiO_2 layer used as reference (black line) were used.

readily observable when the *I–V* curves attained under standard illumination conditions for both cells are compared. In addition to the noticeable increase in photocurrent density for the 1DPC-based DSSC, from 2.81 mA cm^{-2} to 6.06 mA cm^{-2}, the unexpected increase in voltage, from 0.69 V to 0.76 V, leads to an improvement of the overall efficiency up to 140% with respect to the reference cell. Consequently, the solar device based on the periodic photonic structure also shows higher IPCE values, which is in perfect agreement with the measured short circuit photocurrents, as displayed in Figure 4b.

The IPCE efficiency depends on the light harvesting, electron injection, and electron collection efficiencies. Assuming that the collection efficiencies are similar in both the reference and the 1DPC-based cell, we estimated the magnitude of the injection efficiency by using time-correlated single photon counting (TCSPC), as previously described.[29] For both reference and photonic-crystal-based cells, the yield of electron injection was identical and greater than 90%. Thus, the increase in photocurrent can, in principle, only be attributed to the reinforcement of

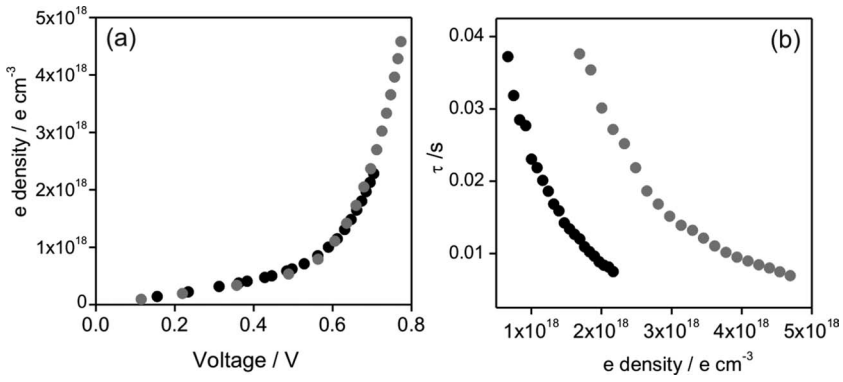

Figure 5. a) Density of charges accumulated at the reference DSSC (black circles) and the 1DPC based DSSC (grey circles) under different light bias estimated from charge extraction measurements. b) Recombination lifetime at different charge density as extracted from transient photovoltage measurements.

optical absorption caused by the specular back reflection from the 1DPC, which acts as a highly efficient dielectric mirror.

On the other hand, the puzzling increase in the cell photovoltage observed for the 1DPC-based DSSC device was further investigated. Interestingly, the dark current versus voltage curves displayed in Figure 4a (black and grey dashed lines for the reference and the 1DPC based cells, respectively) show a similar difference in the value of V_{OC}, which indicates that it has no photonic origin. Thus, we first measured the number of charges present in the device at different light bias by using the charge extraction (CE) technique. The set-up and working principles of the CE technology were reported previously.[30] **Figure 5**a shows the results of the above mentioned experiment. The overlap of the experimental data taken at each different light bias for both cells implies that no shift of the TiO_2 conduction band is appreciated for either the reference cell or that in which the periodic structure has been coupled. As previously described, the voltage in liquid-based DSSCs is set by the energy difference between the Fermi level at the mesoporous semiconductor and the redox potential of the liquid electrolyte. Moreover, the charge recombination reaction between the photoinjected electrons at the TiO_2 and the oxidized species in the electrolyte plays a major role on the open circuit voltage of the cell and, therefore, many studies have been devoted to the influence that the different cell components (dye molecular structure, electrolyte additives, nanoparticle surface coatings, etc.) can have on it.[31,32] The majority of these studies have been carried out by either measuring time-resolved transient photovoltage dynamics (TPV)[33,34] or using impedance spectroscopy (IS).[35–38] In both cases, the results obtained are in perfect agreement, the advantage of the former being the fastest acquisition time, while the latter technique gives information about the charge transfer processes occurring at the Pt counter electrode of the DSSC. We used TPV to measure the charge recombination decays at different light bias for our set of cells. As shown in Figure 5b, the recombination dynamics for the 1DPC based DSSC is slower ($\tau = 40$ ms versus $\tau = 8$ ms corresponding to the reference cell at $n = 1 \times 10^{18}$ electrons cm^{-3}) although under working conditions both devices show a lifetime of 8 ms under 1 sun illumination (maximum charge accumulated at the 1DPC-based device equal to 4.5×10^{18} electrons cm^{-3}, whereas for the reference this value is 1×10^{18} electrons cm^{-3}). Hence, we can conclude that the difference in open circuit voltage on this particular set of devices is due to the slower recombination kinetics between the photoinjected electrons at the TiO_2 and the electrolyte.

It seems feasible that the observed increase in voltage ($\Delta V = 70$ mV) is due to the possible existence of a conformal thin coating of SiO_2 on the surface of the nc-TiO_2 particles of the mesoporous semiconductor film, as it has been reported previously.[27] Salts present in the SiO_2 particle suspension medium, which are extremely difficult to get rid of, would be responsible for the formation of this coating during the deposition of the 1DPC onto the nc-TiO_2 electrode. For other sets of samples containing identical 1DPCs the enhancement in V_{OC} was, however, not so high and systematic. This result is in clear contrast with previous work in which the use of 1DPCs had either no effect or a slightly deleterious one on the value of V_{OC}, very likely as result of poor electrolyte diffusion. Also, it has been observed that this thin layer may also contribute to an increase of the photocurrent.[27] We could confirm that in our cells this effect also occurred and accounted for 10–15% of the total J_{SC} enhancement detected.

As mentioned before, the mechanism of efficiency enhancement when a photonic crystal is integrated in a DSSC has a radically different effect on its transparency than that resulting from the use of diffuse scattering layers. In the case studied here, both devices are fully transparent since the highly porous and nanoparticle-based 1DPC gives rise to no opacity, while, when diffuse scattering layers are employed, all visible wavelengths are strongly scattered at random directions and light not absorbed by the cell is diffusely reflected into the incoming medium. The transmittance and specular reflectance spectra measured for the DSSC based on the photonic crystal layer and for the reference cell are presented in **Figure 6**a,b, respectively. It can be observed in Figure 6a that the use of this type of periodic structure into DSSCs allows a transparent spectral window to be maintained, which can be of interest for applications in building integrated photovoltaics, at the same time that a large rise in the device photocurrent is obtained. Figure 6b displays the specular reflectance spectra of the 1DPC deposited onto the electrode measured, just after the deposition and stabilization of the periodic structure onto the nc-TiO_2 layer (black line) and then for the complete cell (grey line). A high reflectivity Bragg peak, close to 80%, is measured for the electrode coupled to the photonic crystal before the cell assembly. After that, lower reflectance intensity is obtained as a consequence of both the smaller refractive index contrast between SiO_2 and TiO_2 nanoparticle layers when embedded with electrolyte and the presence of a several micrometer thick layer of electrolyte, since the measurement is taken from the counterelectrode side.

Table 1 summarizes the values of all relevant parameters of the DSSCs analyzed here and those in which different TiO_2 film thicknesses have also been used. Interestingly, it can be seen that the benign effect of the photonic crystal deposition on

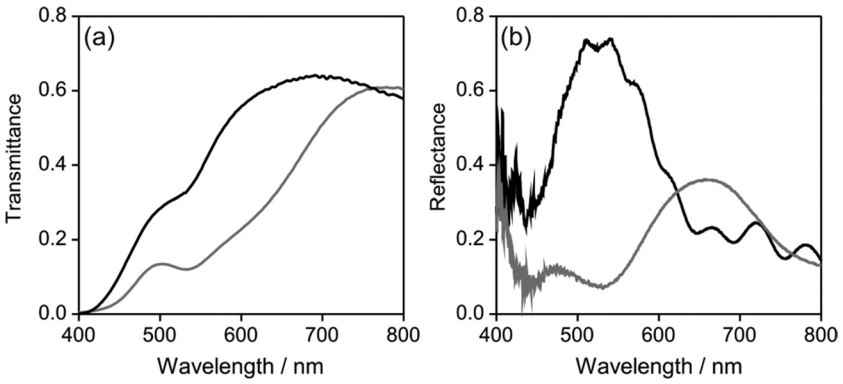

Figure 6. a) Transmittance spectra corresponding to both a DSSC made of a 2 µm thick TiO_2 film coupled to a highly porous 1DPC (grey line) and a reference cell with the same exact thickness of active layer (black line). b) Specular reflectance spectra measured for a 2 µm thick TiO_2 film coupled to a highly porous 1DPC (black line) and for the DSSC including such structure under rear illumination (grey line).

the photovoltage decreases as the thickness of the supporting electrode increases, which might be related to the different way in which the precursors of the extremely thin insulating coating proposed infiltrate the structure as its thickness varies, an effect that has been discussed before.[27] The photovoltage is observed to slightly increase or remain unaltered as the thickness of the electrode is enlarged. Usually devices composed of thicker TiO_2 films show a decrease in photovoltage due to an increase of the recombination kinetics with the electrolyte. Nonetheless, the observed V_{oc} can be explained by the slower recombination dynamics measured when the 1DPC is used at the working electrode (Figure 5b).

3. Conclusions

We have demonstrated that achieving high photocurrent from very thin cells is possible by using highly porous 1DPCs coupled to nc-TiO_2 electrodes. This effect, although less intense, still occurs for thicker cells. We have confirmed that the pore size distribution of the TiO_2 layers in the multilayer affects the diffusion of electrolyte through the cell. Transport of charged species is improved upon increasing of the average pore size and overall porosity in the photonic crystal, which yields better performance of the cell. An unexpected increase of the open circuit photovoltage is also observed for very thin cells, which we could relate to a slower recombination rate as indicated by transient photovoltage measurements that have been realized for the first time in these 1DPC-based DSSCs. The simultaneous increase in both photocurrent and photovoltage boosts the conversion efficiency of thin cells to unprecedented values, close to those typically observed for much thicker ones. At the same time, we have shown that the newly designed photonic crystals perform as light harvesting enhancers, approximately as good as the widely employed diffuse scattering layers, provided that their thickness is on the same order of magnitude, but retaining one of the main advantages of the original cell: its transparency. Further work must be carried out on photonic structures to approach record DSSC efficiencies, but adequate light management, which we have illustrated here, can pave the way to such important goal of making DSSC efficient and transparent for future applications in building integrated photovoltaics.

Table 1. Values attained for the short circuit photocurrent density (J_{SC}), the open circuit photovoltage (V_{OC}), the fill factor (ff), and the power conversion efficiency (η) for several sets of DSSCs with different TiO_2 layer thicknesses.

DSSC	J_{SC} [mA cm^{-2}]	V_{OC} [V]	ff [%]	η [%]
2 µm TiO_2 (Reference)	2.81	0.69	71	1.38
2 µm TiO_2 + 1DPC	6.06	0.76	73	3.37
4 µm TiO_2 (Reference)	7.48	0.77	73	4.21
4 µm TiO_2 + 1DPC	9.85	0.78	67	5.16
4 µm TiO_2 +1 µm scattering layer	9.10	0.77	73	5.15
5 µm TiO_2 (Reference)	9.35	0.79	69	5.10
5 µm TiO_2 + 1DPC	12.13	0.76	68	6.22
5 µm TiO_2 +1 µm scattering layer	11.76	0.77	71	6.50
7 µm TiO_2 (Reference)	12.50	0.77	70	6.80
7 µm TiO_2 + 1DPC	13.43	0.77	67	7.02
7 µm TiO_2 + 1 µm scattering layer	12.87	0.77	73	7.27

4. Experimental Section

Fabrication of TiO_2 Films Coupled to Highly Porous 1DPCs: Before depositing the TiO_2 active layer, the transparent conducting glasses (Nippon Sheet Glass Co, 10 Ω cm^{-2}) were first soaked into a 0.04 M $TiCl_4$ aqueous solution at 70 °C for 15 min and washed with ethanol. Dyesol paste (18NRT) was deposited by a screen printing method to obtain TiO_2 films of different thickness (2, 4, 5, and 7 µm). The resulting electrodes were gradually heated under airflow at 325 °C for 5min, 375 °C for 5 min, 450 °C for 15 min and 500 °C for 15 min. The heated electrodes were soaked again into a 0.04 M $TiCl_4$ aqueous solution at 70 °C for 15 min and then washed with ethanol and dried in air. A TiO_2 paste also containing larger particles (WER2-O, Dyesol) was used to construct a 1 µm thick diffuse scattering layer on the sintered electrodes. In order to fabricate the 1DPC structure on such TiO_2 active layers (0.16 cm^2), an alternated deposition of silica and titania nanoparticles by using a spin-coater (Laurell WS-400E-6NPP) was employed. Silicon oxide particles (20 nm in average size) were purchased from Dupont (LUDOX TMA, 34 wt% suspension in H_2O), whereas nc-TiO_2 particles (6 nm in average size) were synthesized using a procedure previously reported.[39] Both nanoparticle precursors were suspended in a mixture of water (21 vol%) and methanol (79 vol%) using concentrations of 2 wt% SiO_2 and 4 wt% TiO_2, the latter containing a 2 wt% of polymer porogen (PEG 20000, Fluka) for the creation of larger pores within the periodic structure, and concentrations of 2 wt% SiO_2 and 5 wt% TiO_2 for the originally reported photonic crystal. For most cells, Bragg reflectors containing four SiO_2/TiO_2 repeated units were made using 150 µL drops of their respective colloidal suspensions. In this case, both the acceleration ramp and the final rotation speed were fixed at 9180 rpm s^{-1} and 5000 rpm, respectively. Because the spin-coated TiO_2

layers contain a certain amount of organic material incorporated in the dispersion, a thermal stabilization was necessary to avoid dissolving such layer after a subsequent deposition. This heat treatment was performed on a hot plate at 300 °C during 15 min and was repeated following every bilayer (SiO_2/TiO_2) deposition during the multilayer structure formation. After that, all samples were annealed at 450 °C for 30 min to remove organic remains and mechanically stabilize the entire structure.

Optical Characterization of Photoelectrodes: The optical characterization of such porous 1DPCs grown on the nc-TiO_2 electrodes was performed using a Fourier transform infrared spectrophotometer (BRUKER IFS-66) attached to a microscope operating in reflection mode. A 4× objective with a numerical aperture of 0.1 (light cone angle ±5.7°) was used to irradiate the electrode coupled to the photonic crystal and collect the reflected light at quasi-normal incidence with respect to its surface. A spatial filter was used to selectively detect light from 1 mm^2 circular regions of the sample. Optical transmission spectra were also measured with a UV-visible spectrophotometer (UV-2101PC, Shimadzu Corporation).

Preparation and Assembly of DSSCs: TiO_2 photoelectrodes were immersed into a 10^{-3} M C101 dye solution using as solvent a mixture of acetonitrile:tert-butanol (1:1). The counter electrodes were made by spreading a drop of 5×10^{-3} M solution of H_2PtCl_6 in ethanol onto a conducting glass substrate and heated under air flow at 390 °C for 15 min. Both electrodes were sealed using a thermo-polymer (Surlyn). The cells were finally filled with the liquid electrolyte, Z960, through a hole made previously at the back of the platinized counter electrode. Then, the hole was sealed with a thermoplastic polymer and a glass cover slide.

Photovoltaic Characterization: The *I–V* curve measurements were carried out with a 150 W xenon lamp from ABET Instruments with the appropriate filter for the correct simulation of the 1.5 AM G solar spectrum. The incident light power was calibrated using a silicon photodiode previously calibrated at 1000 W m^{-2} at 1.5 AM G. IPCE measurements were carried out with a home-made setup consisting of a 150 W Oriel xenon lamp, a motorized monochromator and a Keithley 2400 digital source meter. An integrating sphere was used to provide homogeneous monochromatic light distribution over the active area of the devices. In addition, the photocurrent and irradiated light intensity were measured simultaneously.

Charge extraction and photovoltage measurements were carried out using a home-built system. In brief, the charge extraction data were acquired using a pulse generated by an array of white LEDs. The decay was monitored using a Tektronics oscilloscope TDS 2022 and recorded using the Tektronics data acquisition software. Different light intensities were applied to achieve different open circuit voltages of the cell and immediately after the light pulse the device was short-circuited to extract the charge. All electronic processes to short-circuit the photovoltaic cell were controlled with a home-made electronic switch. For the photovoltage transients, the pulse was generated with red-emitting diodes while the cell was illuminated with the same array of white light diodes.

Electrochemical Experiments: Diffusion-limited currents within DSSCs were determined by measurement of a cyclic voltammogram (CH Instruments Potentiostat/Galvanostat Model 600D C series) using a slow scan rate of 5 mV s^{-1}. Steady-state conditions were achieved. Thus, the diffusion-limited current density is proportional to the diffusion constant of I^-_3. The diffusion constant was calculated from the following expression:

$$D_{I_3^-} = \frac{j_{lim} l}{2nFc_{I_3^-}} \quad (1)$$

where j_{lim} is the diffusion-limited current, n is the number of electrons, F is the Faraday constant, l the film thickness, and $c_{I_3^-}$ is the molar concentration of triiodide ions.

Acknowledgements

H.M. thanks the Spanish Ministry of Science and Innovation for funding provided under grants MAT2008-02166 and MAT2011-23593, as well as Junta de Andalucía for grants FQM3579 and FQM5247. H.M. and E.P. thank CONSOLIDER HOPE CSD2007-00007. E.P. would like also thanks ICREA and ICIQ for financial support as well as the MICINN for the CTQ2010-18859 and the ERC StG PolyDot projects.

Received: September 12, 2011
Published online: January 23, 2012

[1] C. Y. Chen, M. K. Wang, J. Y. Li, N. Pootrakulchote, L. Alibabaei, C. H. Ngoc-Le, J. D. Decoppet, J. H. Tsai, C. Gratzel, C. G. Wu, S. M. Zakeeruddin, M. Gratzel, *ACS Nano* **2009**, *3*, 3103.
[2] Y. Chiba, A. Islam, Y. Watanabe, R. Komiya, N. Koide, L. Han, *J. Appl. Phys.* **2006**, 45.
[3] F. Gao, Y. Wang, D. Shi, J. Zhang, M. Wang, X. Jing, R. Humphry-Baker, P. Wang, S. M. Zakeeruddin, M. Gratzel, *J. Am. Chem. Soc.* **2008**, *130*, 10720.
[4] S. Ito, S. M. Zakeeruddin, R. Humphry-Baker, P. Liska, R. Charvet, P. Comte, M. K. Nazeeruddin, P. Péchy, M. Takata, H. Miura, S. Uchida, M. Gratzel, *Adv. Mater.* **2006**, *18*, 1202.
[5] A. G. Agrios, I. Cesar, P. Comte, M. K. Nazeeruddin, M. Grätzel, *Chem. Mater.* **2006**, *18*, 5395.
[6] K. M. Lee, V. Suryanarayanan, K. C. Ho, *Sol. Energy Mat. Sol. Cells* **2006**, *90*, 2398.
[7] Z. S. Wang, H. Kawauchi, T. Kashima, H. Arakawa, *Coord. Chem. Rev.* **2004**, *248*, 1381.
[8] F. Huang, D. Chen, X. L. Zhang, R. A. Caruso, Y. B. Cheng, *Adv. Funct. Mater.* **2010**, *20*, 1301.
[9] S. Hore, E. Palomares, H. Smit, N. J. Bakker, P. Comte, P. Liska, K. R. Thampi, J. M. Kroon, A. Hinsch, J. R. Durrant, *J. Mater. Chem.* **2005**, *15*, 412.
[10] M. K. Nazeeruddin, P. Pechy, T. Renourad, S. M. Zakeeruddin, R. Humphry-Baker, P. Comte, P. Liska, L. Cevey, E. Costa, V. Shklover, L. Spiccia, G. B. Deacon, C. A. Bignozzi, M. Gratzel, *J. Am. Chem. Soc.* **2001**, *123*, 1613.
[11] P. Wang, C. Klein, R. Humphry-Baker, S. M. Zakeeruddin, M. Gratzel, *J. Am. Chem. Soc.* **2005**, *127*, 808.
[12] A. Reynal, E. Palomares, *Energy Environ. Sci.* **2010**, *3*, 805.
[13] K. Hara, M. Kurashige, Y. Dan-oh, C. Kasada, A. Shinpo, S. Suga, K. Sayama, H. Arakawa, *New J. Chem.* **2003**, *27*, 783.
[14] C. Y. Chen, S. J. Wu, C. G. Wu, J. G. Chen, K. C. Ho, *Angew. Chem. Int. Ed.* **2006**, *45*, 5822.
[15] J. N. Clifford, E. MArtínez-Ferrero, A. Viterisi, E. Palomares, *Chem. Soc. Rev.* **2011**, *40*, 1635.
[16] J. Liu, R. Li, X. Si, D. Zhou, Y. Shi, Y. Wang, X. Jian, P. Wang, *Energy Environ. Sci.* **2010**, *3*, 1924.
[17] B. E. Hardin, E. T. Hoke, P. B. Armstrong, J. H. Yum, P. Comte, T. Torres, J. M. J. Frechet, M. K. Nazeeruddin, M. Grätzel, M. D. McGehee, *Nat. Photonics* **2009**, *3*, 406.
[18] H. Choi, S. Kim, S. O. Kang, J. Ko, M.-S. Kang, J. N. Clifford, A. Forneli, E. Palomares, M. K. Nazeeruddin, M. Gratzel, *Angew. Chem. Int. Ed.* **2008**, *47*, 8259.
[19] S. Nishimura, N. Abrams, B. A. Lewis, L. I. Halaoui, T. E. Mallouk, K. D. Bekstein, J. van de Lagemaat, A. J. Frank, *J. Am. Chem. Soc.* **2003**, *125*, 6306.
[20] S. Guldin, S. Huttner, M. Kolle, M. E. Welland, P. Müller-Buschbaum, R. H. Friend, N. Steiner, N. Tetreault, *Nano Lett.* **2010**, *10*, 2303.
[21] L. I. Halaoui, N. M. Abrams, T. E. Mallouk, *J. Phys. Chem. C* **2005**, *109*, 6334.

[22] A. Mihi, M. E. Calvo, J. A. Anta, H. Miguez, *J. Phys. Chem. C* **2008**, *112*, 13.
[23] A. Mihi, H. Miguez, *J. Phys. Chem. B* **2005**, *109*, 15968.
[24] S. Colodrero, A. Mihi, L. Haggman, M. Ocaña, G. Boschloo, A. Hagfeldt, H. Miguez, *Adv. Mater.* **2009**, *21*, 764.
[25] G. Lozano, S. Colodrero, O. Caulier, M. E. Calvo, H. Miguez, *J. Phys. Chem. C* **2010**, *114*, 3681.
[26] S. Colodrero, A. Mihi, J. A. Anta, M. Ocaña, H. Miguez, *J. Phys. Chem. C* **2009**, *113*, 1150.
[27] E. Palomares, J. N. Clifford, S. A. Haque, T. Lutz, J. R. Durrant, *J. Am. Chem. Soc.* **2003**, 475.
[28] S. Colodrero, M. Ocaña, H. Miguez, *Langmuir* **2008**, *24*, 4430.
[29] S. A. Haque, E. Palomares, B. M. Cho, A. N. M. Green, N. Hirata, D. R. Klug, J. R. Durrant, *J. Am. Chem. Soc.* **2005**, *127*, 3456.
[30] N. W. Duffy, L. M. Peter, R. M. G. Rajapakse, K. G. U. Wijayantha, *Electrochem. Commun.* **2000**, *2*, 658.
[31] S. A. Haque, Y. Tachibana, R. L. Willis, J. E. Moser, M. Gratzel, D. R. Klug, J. R. Durrant, *J. Phys. Chem. B* **2000**, *104*, 538.
[32] S. Y. Huang, G. Schlichthorl, A. J. Nozik, M. Gratzel, A. J. Frank, *J. Phys. Chem. B* **1997**, *101*, 2576.
[33] T. Dittrich, V. Duzhko, F. Kock, V. Kytin, J. Rappich, *Phys. Rev. B* **2002**, *65*, 155319.
[34] N. Kopidakis, K. D. Benkstein, J. van de Lagemaat, A. J. Frank, *J. Phys. Chem. B* **2003**, *107*, 11307.
[35] J. van de Lagemaat, N. G. Park, A. J. Frank, *J. Phys. Chem. B* **2000**, *104*, 2044.
[36] R. Kern, R. Sastrawan, J. Ferber, R. Stangl, J. Luther, *Electrochim. Acta* **2002**, *47*, 4213.
[37] Q. Wang, J. E. Moser, M. Grätzel, *J. Phys. Chem. B* **2005**, *109*, 14945.
[38] F. Fabregat-Santiago, G. Garcia-Belmonte, J. Bisquert, A. Zaban, P. Salvador, *J. Phys. Chem. B* **2002**, *106*, 334.
[39] S. D. Burnside, V. Shklover, C. Barbe, P. Comte, F. Arendse, K. Brooks, M. Gratzel, *Chem. Mater.* **1998**, *10*, 2419.